The invariant manifolds at infinity of the RTBP and the boundaries of bounded motion

Regina Martínez[(1)] and Carles Simó[(2)]

[(1)] Departament de Matemàtiques, Universitat Autònoma de Barcelona, Bellaterra, Barcelona, Spain
[(2)] Departament de Matemàtica Aplicada i Anàlisi, Universitat de Barcelona, Barcelona, Spain
reginamb@mat.uab.cat, carles@maia.ub.es

Abstract

The invariant manifolds of the periodic orbit at infinity in the planar circular RTBP are studied. To this end we consider the intersection of the manifolds with the passage through the barycentric pericentre. The intersections of the stable and unstable manifolds have a common even part, which can be seen as a displaced version of the two-body problem, and an odd part which gives rise to a splitting. The theoretical formulas, obtained for Jacobi constant C large enough, are compared to direct numerical computations, showing improved agreement when C increases. A return map to the pericentre passage is derived and using an approximation by standard-like maps one can make a prediction of the location of the boundaries of bounded motion. This result is compared to numerical estimates, again improving for C increasing. Several anomalous phenomena are described.

Keywords: invariant rotational curves, separatrix maps, splitting function, Restricted Three Body Problem
MSC: 37N05, 70F07, 37E99

1 Introduction

We consider the planar restricted three-body problem (RTBP) where a negligible mass moves in a plane under the gravitational attraction of two massive bodies of masses $m_1 = 1-\mu, m_2 = \mu$, usually known as primaries, or primary and secondary, for some $\mu \in [0, 1/2)$. We assume that the primaries move in circular orbits around the centre of mass with mean motion and distance between them equal to the unity. It is well known that the motion of the small body can be described, in a fixed reference system (the so-called sidereal system) by a Hamiltonian system defined by

$$H(X_1, X_2, Y_1, Y_2, t) = \frac{1}{2}(Y_1^2 + Y_2^2) - \left(\frac{1-\mu}{r_1} + \frac{\mu}{r_2}\right), \tag{1}$$

where (X_1, X_2) is the position of the small body in an inertial frame and

$$r_1^2 = (X_1 - \mu\cos(t))^2 + (X_2 - \mu\sin(t))^2, \quad r_2^2 = (X_1 + (1-\mu)\cos(t))^2 + (X_2 + (1-\mu)\sin(t))^2.$$

The system defined by (1) has two degrees of freedom and it is periodically time-dependent. However it has a well known conserved quantity, the so-called Jacobi integral, defined as twice the difference between angular momentum and energy

$$C = 2(M - H), \quad M = X_1Y_2 - X_2Y_1 \quad \text{and } H \text{ as in (1)}. \tag{2}$$

It is often defined C by adding to (2) the value $\mu(1-\mu)$ so that at the relative equilibrium solutions $L_{4,5}$ the value of C equals 3. But in what follows we shall use the value defined by

(2). Given a value $C > 0$, large enough, the motion is confined to the so-called Hill's regions, either around some of the massive bodies or in the outer region, away from both of them. Here we consider the motion in the outer case.

It is clear that for small values of μ, the problem can be seen as a perturbation of the two-body problem, that is $H(X_1, X_2, Y_1, Y_2, t) = H_0(X_1, X_2, Y_1, Y_2) + H_1(X_1, X_2, Y_1, Y_2, t)$, where $H_0(X_1, X_2, Y_1, Y_2) = \frac{1}{2}(Y_1^2 + Y_2^2) - 1/r$, $r = \sqrt{X_1^2 + X_2^2}$ and $H_1 = O(\mu)$. Note that H_0 is autonomous.

In the two-body problem there are parabolic orbits on the zero level of energy $H_0 = 0$, going to infinity for $t \to \pm\infty$ with zero limit velocity. The limit point can be seen as a fixed point in suitable coordinates [10], see Sect. 2, which is of parabolic type, i.e. with zero eigenvalues. The parabolic orbits can be seen as stable, W^s_∞, and unstable, W^u_∞, manifolds of that point and, obviously, they coincide.

Passing to the RTBP one has to include the 2π periodic effect of t. As shown in Sect. 2 this is equivalent to consider a periodic orbit at infinity [11]. The interesting fact is that in that case the manifolds do not longer coincide, as already shown by Moser [11] in the case of the Sitnikov problem [15]. This lack of coincidence leads to several well-known facts: non-integrability, existence of symbolic dynamics and oscillatory solutions, escape and capture domains, etc.

At some distance of the manifolds one can expect to be able to prevent from escape. This can be seen, in a suitable Poincaré section, as existence of invariant rotational curves (IRC) confining the dynamics under the related Poincaré map. This topic has been considered in [8] for the Sitnikov problem.

The goal of this paper is double. Here we present both of them, the related sections of the paper and a short sample of references:

1) To study the behaviour of the invariant manifolds of the periodic orbit at infinity and how they depend on C and μ. This problem has been approached in several papers like [6] (for large C and very small μ), [7] (for the planar elliptic problem) and, recently, [5] (without the smallness condition on μ). These questions will be considered in Sect. 2 concerning the local expression of the manifolds close to infinity, with details in the Appendix, and in Sect. 3 concerning the first intersections with a suitable Poincaré map.

   A typical problem in this kind of topics is the domain of validity in the parameters (μ, C). Some preliminary numerical results where given in [6]. In Sect. 4 a systematic study is carried out, allowing to detect different kinds of anomalies.

2) To detect the existence of boundaries preventing escape (and capture) as a function of (μ, C). In principle, for large C, it is possible to look for a return map to the selected Poincaré section, following the ideas of Chirikov, Zaslavskii and coworkers [18, 1], and more recent approaches by Treschev and coworkers [17, 14].

   These return maps depend on the splitting function, which measures the lack of coincidence of W^u_∞ and W^s_∞ on a Poincaré section. They are of the so-called separatrix map type and they can be approximated, in suitable domains, by standard-like maps. See [8] for an expository work in this direction. When the approximation provided by the classical standard map (that is, the periodic function is assumed to have a shape like $\sin(\theta)$) is good enough, IRC exist for parameter values below the well-known Greene value, $\kappa_G \approx 0.971635$, see [4]. This can be suitable for large values of C and μ outside a domain of the form $(\mu^*(C), 1/2)$, where $\mu^*(C) \to 1/2$ as $C \to \infty$, see Sect. 3.

   Decreasing the value of C or in the domain excluded in the previous paragraph, the splitting function has important contributions from two harmonics with a shape, say, of the form $\cos(2\pi\gamma)\sin(\theta) + \sin(2\pi\gamma)\sin(2\theta)$, where it is enough to consider $\gamma \in (-1/4, 1/4]$. These terms show up in the related standard-like map and, then, the corresponding Greene-like value depends on the parameter γ. Values of $\kappa_G(\gamma)$ between 0.330 and 1.888, with a wild dependence in γ in some ranges, have been observed. See [8] for full details. It is worth to mention related results in [2], looking for IRC with given noble rotation numbers for several families of standard-like maps.

A summary of results and theoretical predictions on the location of IRC for large C is presented in Sect. 5. But for decreasing C, and depending also on the value of μ, one has to do numerical estimates of the IRC closest to the invariant manifolds of the periodic orbits at infinity. A methodology and a sample of results are given in Sect. 6.

An interesting complementary work, to show the existence of instabilities in the RTBP, based on Aubry-Mather theory, can be found in [3].

As mentioned it is useful to introduce a Poincaré section Σ to see how the manifolds intersect it and to locate IRC preventing from escape. Along the paper we use as Σ the section defined by the passage through the pericentre:

$$\Sigma = \{(X_1, X_2, Y_1, Y_2, t) \in \mathbb{R}^5 \mid r = (X_1^2 + X_2^2)^{1/2} \text{ is at a local minimum with respect to } t\}. \quad (3)$$

In the case of the two-body problem, for a given C and energy $H_0 = h$ the value of r at the pericentre is given by $r_p = C^2/8$. We note, however, that some irregular behaviour appears when trying to obtain r_p for h close to 0. From $M = C/2 + h$ and using $M = r_p v_p$, where v_p denotes the velocity at the pericentre, one has $h = (C/2 + h)^2/(2r_p^2) - 1/r_p$, which allows to determine r_p. Let us write $r_p = C^2/8 + \Delta$, which leads to

$$\left(\frac{C^4}{64} - \frac{C}{2}\right) h + \Delta - \frac{h^2}{2} + \frac{C^2}{4} h\Delta + h\Delta^2 = 0.$$

It is clear that for the critical value $C = C_c = 32^{1/3}$ the behaviour of Δ around $h = 0$ is $\Delta = h^2/2 + \mathcal{O}(h^3)$, while it is $\Delta = -(C^4/64 - C/2)h + \mathcal{O}(h^2)$ for $C \neq C_c$. For $C > C_c$ the function Δ has a minimum (< 0) for $h > 0$, while for $C < C_c$ the minimum is also < 0 but it is achieved for $h < 0$. In particular, for $h < 0$ and $|h|$ small, $\Delta > 0$ (resp. $\Delta < 0$) if $C > C_c$ (resp. $C < C_c$). This change of local behavior in the shift of r_p as a function of h for h small, depending on C, will produce several anomalous effects on the intersections of the manifolds with Σ and in the splitting, as it will be shown on Sect. 4.

2 Invariant manifolds at infinity

In a rotating frame (the synodical frame), so that the primaries are kept fixed at $(\mu, 0)$ and $(\mu - 1, 0)$, the equations of motion (see [16]) become

$$\ddot{x} - 2\dot{y} = \frac{\partial \Omega}{\partial x}, \qquad \ddot{y} + 2\dot{x} = \frac{\partial \Omega}{\partial y},$$

where

$$\Omega(x, y) = \frac{1}{2}(x^2 + y^2) + \frac{1-\mu}{r_1} + \frac{\mu}{r_2}$$

and $r_1^2 = (x - \mu)^2 + y^2$ and $r_2^2 = (x + 1 - \mu)^2 + y^2$. The Jacobi integral becomes

$$C = 2\Omega(x, y) - (\dot{x}^2 + \dot{y}^2)$$

and its value is denoted as the Jacobi constant. We refer to (2) for the expression and meaning in a fixed frame.

Following [6] to study the motion near infinity we introduce McGehee coordinates q, p, θ, ω (see [10]) in the following way

$$x + \mathrm{i}\, y = \frac{2}{q^2} e^{\mathrm{i}\,\theta}, \qquad \dot{x} + \mathrm{i}\, \dot{y} = \left(p + \mathrm{i}\, \left(q^2\omega/2 - 2/q^2\right)\right) e^{\mathrm{i}\,\theta}$$

with $q \in (0, \infty)$. Notice that $\omega = X_1 Y_2 - X_2 Y_1$ is the angular momentum, denoted as M in (2). It is also clear that if we denote as α the argument of the position of the body of negligible mass in the sidereal system (i.e. $X_1 = r\cos(\alpha), X_2 = r\sin(\alpha)$), then $\theta = \alpha - t$. This will be used in Sect. 6. Using the new variables the equations of motion are

$$\begin{aligned}
\dot{q} &= -\frac{1}{4} q^3 p, \\
\dot{p} &= -\frac{1}{4} q^4 + \frac{1}{8} q^6 \omega^2 + \frac{1}{4} q^4 (1 - \sigma_3) + \frac{\mu(1-\mu)}{8} q^6 \sigma_2 \cos\theta, \\
\dot{\theta} &= -1 + \frac{1}{4} q^4 \omega, \\
\dot{\omega} &= -\frac{\mu(1-\mu)}{4} q^4 \sigma_2 \sin\theta
\end{aligned} \tag{4}$$

and the Jacobi integral is written as

$$C = q^2 - p^2 + 2\omega - \frac{1}{4} q^4 \omega^2 + q^2(\sigma_1 - 1), \tag{5}$$

where

$$\sigma_1 = \frac{1-\mu}{f_\mu} + \frac{\mu}{f_{\mu-1}}, \quad \sigma_2 = \frac{1}{f_\mu^3} - \frac{1}{f_{\mu-1}^3}, \quad \sigma_3 = \frac{1-\mu}{f_\mu^3} + \frac{\mu}{f_{\mu-1}^3}, \tag{6}$$

being

$$f_m = \left(1 - m q^2 \cos\theta + \frac{m^2}{4} q^4\right)^{1/2}.$$

Notice that the values defined in (6) satisfy $\sigma_1 = 1 + O(q^4)$, $\sigma_2 = O(q^2)$ and $\sigma_3 = 1 + O(q^4)$.

For a fixed value of C, the system (4) is well defined at $q = 0$ and it has a periodic orbit, OP_∞, given by $q = 0, p = 0, \omega = C/2, \theta \in \mathbb{S}^1$, which corresponds to the motion of the primaries. It is well known that OP_∞ has two dimensional stable (W^s_∞) and unstable (W^u_∞) invariant manifolds on $q \geq 0$. In fact, once C is fixed, it is possible to eliminate ω in (4) using (5) giving rise to a new system for q, p, θ. Using a suitable Poincaré map, OP_∞ becomes a parabolic fixed point $q = 0, p = 0$, which has stable and unstable invariant manifolds (see [10]). The invariant manifolds are analytic, and with analytic dependence on parameters on a suitable compact set, in an open domain around $q = 0, p = 0$, except at the origin itself. In the case of a similar problem, the Sitnikov problem [15], it is proved that, around the origin $q = 0, p = 0$ the invariant manifolds are exactly of Gevrey class 1/3 (see [9]) for eccentricity of the primaries $e \in (0, 1]$. One can conjecture the same result in present case for $\mu \in (0, 1)$ and any value of C, but this is beyond the scope of the present work.

We look for a local expression of W^s_∞, for $q > 0$ small, of the form

$$p = F(q, \theta) = \sum_{j \geq 1} a_j(\theta) q^j = q + \dots, \tag{7}$$

where $a_j(\theta)$ are periodic functions in θ. We note that using the symmetry $(q, p, \theta, \omega, t) \to (q, -p, -\theta, \omega, -t)$, we have $p = -F(q, -\theta)$ for W^u_∞.

The methodology to compute the coefficients $a_j(\theta)$, $j \geq 2$ in a recurrent way is given in the Appendix. The first ones are

$$a_2(\theta) = a_4(\theta) = a_6(\theta) = a_7(\theta) = a_9(\theta) = 0, \quad a_3(\theta) = -\frac{C^2}{2^5},$$

$$a_5(\theta) = \frac{\mu(1-\mu)}{2^5} - \frac{C^4}{2^{11}}, \quad a_8(\theta) = \frac{9\mu(1-\mu)}{2^7}\sin(2\theta).$$

In the integrable case $\mu = 0$, ω is constant and $\omega = C/2$ for OP_∞. Then the invariant manifolds $W^{s,u}_\infty$ are exactly $p = \pm q\sqrt{1 - q^2C^2/16}$. In this case, as expected, W^s_∞ and W^u_∞ coincide.

3 The infinity manifolds on the pericentre passage and the related splitting

For concreteness we shall consider in this section $C > C_c = 32^{1/3}$.

For a fixed value of C we consider the section $\Sigma = \{q, p, \theta, \omega) \mid$ they satisfy $(5), p = 0\}$ corresponding to the passage of orbits through the pericentre. It is equivalent to (3) in the McGehee coordinates. In Σ we take q, θ as polar coordinates and ω is recovered from (5).

In the case $\mu = 0$, $W^s_\infty \cap \Sigma = W^u_\infty \cap \Sigma$ is a circle of radius $q = 4/C$. The points in Σ with $q < 4/C$ correspond to elliptic orbits of the two-body problem.

For $\mu > 0$, W^s_∞ and W^u_∞ do not coincide. If μ is small enough it is expected that they intersect Σ in two curves near the circle above. In fact, if $W^s_\infty \cap \Sigma$ is given by some function $q = 4/C + g^s(\theta; \mu, C)$ (in polar coordinates) then $W^u_\infty \cap \Sigma$ is given by $q = 4/C + g^u(\theta; \mu, C)$ with $g^u(\theta; \mu, C) = g^s(-\theta; \mu, C)$. Therefore these two curves intersect at $\theta = 0$ and $\theta = \pi$ giving rise to orbits which escape parabolically to infinity for positive and negative time.

Our purpose is to compute a first approximation of $g^s(\theta; \mu, C)$ for $\mu > 0$ small enough. In other words, we neglect in this section the $\mathcal{O}(\mu^2)$ terms. To do that we shall follow the main steps used in [7] for the planar elliptic restricted three-body problem. We note that in [7] the main interest was to compute the splitting, that is, the difference between g^u and g^s. Now we are interested in the full expression of these intersections, to find the displacement of $g^{s,u}$ with respect to the two-body problem case. We rely on some of the results proved in [7].

We introduce $\mathbf{z} = (q, p, \theta, \omega)$ and write the equations (4) as

$$\dot{\mathbf{z}} = F_0(\mathbf{z}) + \mu F_1(\mathbf{z}) + F_2(\mathbf{z}, \mu), \tag{8}$$

where

$$\begin{aligned} F_0(\mathbf{z}) \;&=\; (-\frac{1}{4}q^3p,\, -\frac{1}{4}q^4 + \frac{1}{8}q^6\omega^2,\, -1 + \frac{1}{4}q^4\omega,\, 0), \qquad F_1(\mathbf{z}) = (0,\, G_1,\, 0,\, G_2), \\ & G_1(q,\theta) = \left(\frac{q^4}{4} + \frac{q^6}{8}\cos\theta\right)\left(1 - \frac{1}{R^3}\right) - \frac{3}{8}q^6\cos\theta, \quad G_2(q,\theta) = -\frac{1}{4}q^4\sin\theta\left(1 - \frac{1}{R^3}\right), \\ & R(q,\theta) = (1 + q^2\cos\theta + \frac{1}{4}q^4)^{1/2} \end{aligned}$$

and $F_2(\mathbf{z}, \mu)$ is a function of order 2 in μ. Let $\mathbf{z}(t; \mathbf{z}_i, \mu)$ be the solution of (8) such that $\mathbf{z}(0; \mathbf{z}_i, \mu) = \mathbf{z}_i$. For a fixed value of C we look for initial conditions $\mathbf{z}_i = \mathbf{z}_0 + \mu(\Delta q, 0, 0, \Delta\omega) + \mathcal{O}(\mu^2)$ where $\mathbf{z}_0 = (q_0, 0, \theta_0, \omega_0)$, with $q_0 = 4/C, \omega_0 = C/2$, such that the corresponding orbit belongs to W^s_∞. We note that once C is fixed, $C^3 \neq 32$, Δq and $\Delta\omega$ are not independent. In fact using (5) one has

$$\Delta\omega = \frac{C^2}{C^3 - 32}\left(4\Delta q + \frac{8}{C}\left(1 - \frac{1}{R(q_0,\theta_0)} - \frac{8}{C^2}\cos\theta_0\right)\right) + O(\mu). \tag{9}$$

We shall write

$$\mathbf{z}(t;\mathbf{z}_i,\mu)=\mathbf{z}(t;\mathbf{z}_0,0)+\mu\mathbf{z}_b(t;\Delta q)+O(\mu^2)$$

where $\mathbf{z}(t;\mathbf{z}_0,0)=(\hat{q}(t),\hat{p}(t),\hat{\theta}(t),\omega_0)$ is the solution of the two-body problem and $\mathbf{z}_b$ is the solution of the variational equations

$$\begin{aligned}\dot{\mathbf{z}}_b &= DF_0(\mathbf{z}(t;\mathbf{z}_0,0))\mathbf{z}_b+F_1(\mathbf{z}(t;\mathbf{z}_0,0)),\\ \mathbf{z}_b(0) &= (\Delta q,0,0,\Delta\omega).\end{aligned}\tag{10}$$

Following [7] we introduce a new time τ through $dt/d\tau=2\omega_0/\hat{q}^2$. Then

$$\hat{q}(\tau)=\frac{2}{\omega_0(1+\tau^2)^{1/2}},\quad \hat{p}(\tau)=\frac{2\tau}{\omega_0(1+\tau^2)},\quad \hat{\theta}(\tau)=\theta_0+2\arctan\tau-\frac{\omega_0^3}{2}\left(\tau+\frac{\tau^3}{3}\right)\tag{11}$$

and the equations (10) become

$$\begin{aligned}q_b' &= \left(-\frac{3}{2}\omega_0\hat{p}\right)q_b-\left(\frac{\omega_0}{2}\hat{q}\right)p_b,\\ p_b' &= \left(-2\omega_0\hat{q}+\frac{3}{2}\omega_0^3\hat{q}^3\right)q_b+g(\tau),\qquad g(\tau)=\left(\frac{\omega_0^2}{2}\hat{q}^4\right)\omega_b+\frac{2\omega_0}{\hat{q}^2}G_1(\hat{q},\hat{\theta}),\\ \theta_b' &= \left(2\omega_0^2\hat{q}\right)q_b+\left(\frac{\omega_0}{2}\hat{q}^2\right)\omega_b,\\ \omega_b' &= \frac{2\omega_0}{\hat{q}^2}G_2(\hat{q},\hat{\theta}).\end{aligned}\tag{12}$$

We can reduce to consider in (12) the equations for q_b and p_b because ω_b is obtained by integration and θ_b could be also determined once the other variables are known. Therefore, using (11) we get the following non homogeneous linear system

$$\begin{aligned}&q_b'-\frac{3\tau}{1+\tau^2}q_b-\frac{1}{(1+\tau^2)^{1/2}}p_b,\qquad p_b'=\left(-\frac{4}{(1+\tau^2)^{1/2}}+\frac{12}{(1+\tau^2)^{3/2}}\right)q_b+g(\tau),\\ &q_b(0)=\Delta q,\qquad p_b(0)=0.\end{aligned}\tag{13}$$

A fundamental system of solutions for the homogeneous system associated to (13) is known (see [7]). Moreover, it is proved in [7] that if ω_0 is large enough and

$$\Delta q=-\int_0^\infty\frac{\tau}{1+\tau^2}g(\tau)d\tau,\tag{14}$$

then the solution of (13) satisfies that $q_b(\tau)$ and $p_b(\tau)$ go to 0 as $\tau\to\infty$. To compute Δq in the present case we write the integral in (14) as

$$\Delta q=-\frac{2}{\omega_0^2}\Delta\omega-\int_0^\infty\left(\frac{\omega_0}{(1+\tau^2)}G_2+\frac{\omega_0^3\tau}{2}G_1\right)d\tau,$$

where G_1,G_2 are evaluated on the solution of the two-body problem (11). Using (9) we obtain

$$\Delta q=\frac{64}{C^4}\left(-1+\frac{8}{C^2}\cos\theta_0+\frac{1}{R(q_0,\theta_0)}\right)-\frac{(C^3-32)}{C^3}\int_0^\infty\left(\frac{\omega_0}{(1+\tau^2)}G_2+\frac{\omega_0^3\tau}{2}G_1\right)d\tau.$$

We note that Δq is a 2π-periodic function on θ_0 whose coefficients depend on C. Let $g_c^s(\mu,C)$ be the constant part of $\mu\Delta q+\mathcal{O}(\mu^2)$ and $g_e^s(\theta_0;\mu,C),g_o^s(\theta_0;\mu,C)$ be the even and odd parts, with respect to θ_0, of the purely periodic part of $\mu\Delta q+\mathcal{O}(\mu^2)$, respectively. The following lemma gives the dominant terms for large values of C.

Lemma 3.1. *If C is large enough, then*

$$g^s_c(\mu, C) = \mu\left(\frac{32}{C^5} + O_9\right) + \mathcal{O}(\mu^2),$$

$$g^s_e(\theta_0;\mu, C) = \mu\left[\cos(\theta_0)\left(\frac{3\cdot 2^{18}}{C^{13}} + O_{16}\right) + \cos(2\theta_0)\left(-\frac{9\cdot 2^{12}}{C^{11}} + O_{14}\right) + \dots\right] + \mathcal{O}(\mu^2),$$

$$g^s_o(\theta_0;\mu, C) = \mu\left[\sin(\theta_0)\exp(-C^3/24)\left(-\frac{\sqrt{\pi}}{16}C^{1/2} + \dots\right) + \sin(2\theta_0)\exp(-C^3/12)\left(\frac{\sqrt{2\pi}}{4}C^{5/2} + \dots\right)\right] + \mathcal{O}(\mu^2),$$

where O_k stands for terms of order k in C^{-1}.

Proof. Let us introduce

$$U(\theta_0, C) := \frac{64}{C^4}\left(-1 + \frac{8}{C^2}\cos\theta_0 + \frac{1}{R(q_0, \theta_0)}\right),$$

$$V(\theta_0, C) := \frac{(C^3 - 32)}{2C^2}\int_0^\infty \mathcal{B}(\tau, \hat\theta(\tau), C)d\tau, \qquad \mathcal{B}(\tau, \hat\theta(\tau), C) = \frac{1}{(1+\tau^2)}G_2 + \frac{C^2\tau}{8}G_1.$$

Then $\Delta q = U(\theta_0, C) - V(\theta_0, C)$. Is is easy to check that the constant part of U, is

$$U_c(C) = \frac{2^{10}}{C^8} + \frac{9\cdot 2^{12}}{C^{12}} + \dots\ . \tag{15}$$

Moreover for the even part we obtain

$$U_e(\theta_0, C) = \cos\theta_0\left[-\frac{3\cdot 2^{12}}{C^{10}} - \frac{15\cdot 2^{15}}{C^{14}} + O_{18}\right] + \cos(2\theta_0)\left[\frac{3\cdot 2^{10}}{C^8} + \frac{5\cdot 2^{14}}{C^{12}} + O_{16}\right] + \mathcal{U}(\theta_0, C), \tag{16}$$

where $\mathcal{U}(\theta_0, C)$ contain terms in $\cos(j\theta_0)$ with $j \geq 3$.

To compute the corresponding terms for $V(\theta_0, C)$ first, we expand $\mathcal{B}$ as

$$\mathcal{B}_0(\tau, C) + \mathcal{B}_{c1}(\tau, C)\cos\hat\theta + \mathcal{B}_{s1}(\tau, C)\sin\hat\theta + +\mathcal{B}_{c2}(\tau, C)\cos(2\hat\theta) + \mathcal{B}_{s2}(\tau, C)\sin(2\hat\theta) + \dots,$$

with

$$\begin{aligned}
\mathcal{B}_0(\tau, C) &= -\frac{3\cdot 2^7\tau}{C^6(1+\tau^2)^4} - \frac{45\cdot 2^9\tau}{C^{10}(1+\tau^2)^6} + \dots,\\
\mathcal{B}_{c1}(\tau, C) &= \frac{3\cdot 2^{11}\tau}{C^8(1+\tau^2)^5} + \frac{45\cdot 2^{13}\tau}{C^{12}(1+\tau^2)^7} + \dots,\\
\mathcal{B}_{s1}(\tau, C) &= \frac{3\cdot 2^9}{C^8(1+\tau^2)^5} + \frac{15\cdot 2^{12}}{C^{12}(1+\tau^2)^7} + \dots,\\
\mathcal{B}_{c2}(\tau, C) &= -\frac{9\cdot 2^7\tau}{C^6(1+\tau^2)^4} - \frac{25\cdot 2^{11}\tau}{C^{10}(1+\tau^2)^6} + \dots,\\
\mathcal{B}_{s2}(\tau, C) &= -\frac{3\cdot 2^8}{C^6(1+\tau^2)^4} - \frac{5\cdot 2^{12}}{C^{10}(1+\tau^2)^6} + \dots\ .
\end{aligned}$$

The constant terms of $V(\theta_0, C)$ are

$$\frac{(C^3 - 32)}{2C^2}\int_0^\infty \mathcal{B}_0(\tau, C)d\tau = \frac{(C^3 - 32)}{2C^2}\left(-\frac{2^6}{C^6} - \frac{9\cdot 2^8}{C^{10}} + \dots\right) = -\frac{2^5}{C^5} + \frac{2^{10}}{C^8} - \frac{9\cdot 2^7}{C^9}\dots\ .$$

Then, using (15) we obtain the constant part g_c^s of Δq.

In order to compute the periodic part of $V(\theta_0, C)$, first we use (11) to expand $\cos\hat{\theta}, \sin\hat{\theta}$, $\cos(2\hat{\theta}), \sin(2\hat{\theta})$ in terms of θ_0, τ and $(\omega_0^3/2)(\tau + \tau^3/3)$. Then, we collect the terms in $\sin\theta_0$ and $\cos\theta_0$ from $\mathcal{B}_{c1}(\tau, C)\cos\hat{\theta} + \mathcal{B}_{s1}(\tau, C)\sin\hat{\theta}$ and the terms in $\sin(2\theta_0)$ and $\cos(2\theta_0)$ from $\mathcal{B}_{c2}(\tau, C)\cos(2\hat{\theta}) + \mathcal{B}_{s2}(\tau, C)\sin(2\hat{\theta})$.

It turns out that the contribution of these terms to $\int_0^\infty \mathcal{B} d\tau$ can be written in terms of the following integrals, depending on a real parameter δ:

$$
\begin{aligned}
I_k(\delta) + \mathrm{i}\, J_k(\delta) &= \int_0^\infty \frac{\exp(\mathrm{i}\,\delta(\tau + \tau^3/3))}{(1+\tau^2)^k} d\tau, \\
N_k(\delta) + \mathrm{i}\, M_k(\delta) &= \int_0^\infty \frac{\tau\, \exp(\mathrm{i}\,\delta(\tau + \tau^3/3))}{(1+\tau^2)^k} d\tau.
\end{aligned}
$$

More precisely

$$
\begin{aligned}
&\int_0^\infty [\mathcal{B}_{c1}(\tau, C)\cos\hat{\theta} + \mathcal{B}_{s1}(\tau, C)\sin\hat{\theta}] d\tau = \\
&\cos\theta_0 \left(\frac{3\cdot 2^9}{C^8}[10N_6(\gamma) - 4N_5(\gamma) - 10J_6(\gamma) - 9J_5(\gamma)] \right. \\
&\left. + \frac{15\cdot 2^{12}}{C^{12}}[14N_8(\gamma) - 6N_7(\gamma) - 14J_8(\gamma) + 13J_7(\gamma)] + \dots \right) + \\
&\sin\theta_0 \left(\frac{3\cdot 2^9}{C^8}[-9I_5(\gamma) + 10I_6(\gamma) - 4M_5(\gamma) + 10M_6(\gamma)] + \right. \\
&\left. \frac{15\cdot 2^{12}}{C^{12}}[-13I_7(\gamma) + 14I_8(\gamma) - 6M_7(\gamma) + 14M_8(\gamma)] + \dots \right),
\end{aligned}
$$

where $\gamma = \omega_0^3/2 = C^3/16$. In a similar way one has

$$
\begin{aligned}
&\int_0^\infty [\mathcal{B}_{c2}(\tau, C)\cos(2\hat{\theta}) + \mathcal{B}_{s2}(\tau, C)\sin(2\hat{\theta})] d\tau = \\
&\cos(2\theta_0) \left(-\frac{3\cdot 2^7}{C^6}[40N_6(2\gamma) - 32N_5(2\gamma) + 3N_4(2\gamma) - 40J_6(2\gamma) + 52J_5(2\gamma) - 14J_4(2\gamma)] \right. \\
&\left. - \frac{5\cdot 2^{11}}{C^{10}}[56N_8(2\gamma) - 48N_7(2\gamma) + 5N_6(2\gamma) - 56J_8(2\gamma) + 76J_7(2\gamma) - 22J_6(2\gamma)] \dots \right) \\
&\sin(2\theta_0) \left(\frac{3\cdot 2^7}{C^6}[-14I_4(2\gamma) + 52I_5(2\gamma) - 40I_6(2\gamma) - 3M_4(2\gamma) + 32M_5(2\gamma) - 40M_6(2\gamma)] + \right. \\
&\left. + \frac{5\cdot 2^{11}}{C^{10}}[-22I_6(2\gamma) + 76I_7(2\gamma) - 56I_8(2\gamma) - 5M_6(2\gamma) + 48M_7(2\gamma) - 56M_8(2\gamma)] + \dots \right).
\end{aligned}
$$

In [7] it is proved that if $\delta > 0$ is large enough, then for any $k > 0$ the following formulas hold

$$
J_k(\delta) = \delta^{-1} + 2(k+1)\delta^{-3} + 4(k+1)(3k+10)\delta^{-5} + O(\delta^{-7}), \tag{17}
$$

$$
N_{k+2}(\delta) = \frac{1}{2(k+1)}[1 - \delta J_k(\delta)] = -\delta^{-2} - 2(3k+10)\delta^{-4} + O(\delta^{-6}), \tag{18}
$$

$$
M_{k+2}(\delta) = \frac{\delta}{2(k+1)} I_k(\delta). \tag{19}
$$

Moreover (see [7]) asymptotic expansions are obtained for $I_k(\delta)$. For $n \geq 2$ the results in [7] can be summarized as

$$\begin{aligned}
I_{2n-1}(\delta) &= \exp(-2\delta/3)\left[\frac{\pi}{2^{n+1}(2n-2)!!}\delta^{n-1}+O(\delta^{n-3/2})\right],\\
I_{2n}(\delta) &= \exp(-2\delta/3)\left[\frac{\sqrt{\pi}}{2^{n+1}(2n-1)!!}\delta^{n-1/2}+O(\delta^{n-1})\right].
\end{aligned}\tag{20}$$

The asymptotic expansions (17) and (18) allows us to compute the dominant terms in the coefficients of $\cos(\theta_0)$ and $\cos(2\theta_0)$ in $V(\theta_0, C)$. Therefore we have the following terms for the even part of the V

$$V_e(\theta_0, C) := \cos\theta_0\left[-\frac{3\cdot 2^{12}}{C^{10}}-\frac{3\cdot 2^{18}}{C^{13}}-\frac{15\cdot 2^{15}}{C^{14}}-\frac{15\cdot 2^{22}}{C^{16}}+\dots\right]+$$

$$+\cos(2\theta_0)\left[\frac{3\cdot 2^{10}}{C^{8}}+\frac{9\cdot 2^{12}}{C^{11}}+\frac{5\cdot 2^{14}}{C^{12}}+\frac{3\cdot 2^{20}}{C^{14}}\dots\right]+\dots$$

Then using (15) and (16) $g_e^s(\theta_0, C)$ is easily obtained. The odd part of $V(\theta_0, C)$ and hence, $g_o^s(\theta_0, C)$, is obtained using (20) and (19). □

Remark 3.1. *As mentioned at the beginning of this section, the terms $\mathcal{O}(\mu^2)$ are neglected. It can not be excluded that there appear other terms containing μ^2 as a factor and which are multiplied by* $\exp(-C^3/24)$ *in the expression of g_o^s given in the Lemma. They will be larger than the terms which appear in* $\mu\exp(-C^3/12)$ *provided μ is not very small. In fact this do happens, as we shall see in Sect. 4.*

4 Numerical computation of the invariant manifolds

From the results in Sect. 2 we have local expressions of the manifolds around $(q, p) = (0, 0)$ and the results of Sect. 3 predict the behaviour of the intersections of the manifolds with the Poincaré section Σ.

The results of Sect. 3 hold for C sufficiently large. So, it is interesting to see the behaviour of the invariant manifolds for a wide range of values of C, not necessarily large, using numerical computations. The procedure is as follows:

a) Given (μ, C), a value of q and an angle θ one computes p from (7) using the coefficients obtained as explained in the Appendix. If the initial point is in W^s_∞ one should integrate back in time.

   A first question is how to select a suitable q. This is easily solved by using the methods in [13]. Take a rather small value of q, say q_1 and an initial angle θ_1. Compute the corresponding values p_1, ω_1 and proceed to integrate (4). After several integration steps one has new values $(q_2, p_2, \theta_2, \omega_2)$ and one can check if the values of p_2, ω_2 agree, with a prescribed tolerance, with the ones obtained from the local expansions using q_2, θ_2. Typically in the computations one has used $q = 0.04$ for double precision and $q = 0.02$ for higher precision. They are enough for the ranges of (μ, C) used in the computations.

   The integration of the ODE in all cases have been done using high order Taylor methods.

b) Then one takes a suitable initial value of q, equispaced initial values of the angle θ, $\theta_i \in [0, 2\pi]$ (e.g. 2^{12} values) and for each one we proceed to integrate (4) until arriving to Σ, at the first passage of p through 0. One looks at the result as q, shifted by $4/C$, as being a graph on θ, $q - 4/C = g^s(\theta)$ in the case of W^s_∞, as done in Sect. 3. For values of (μ, C) with C close to 3 and even $C < 3$ either q is no longer a graph depending on θ or there are discontinuities in the final point as a function of θ_i. This is due to passages relatively close to a primary. These cases are discarded.

c) The function g^s is Fourier analyzed, obtaining a representation of the form

$$g^s(\theta) = g_c^s + g_e^s + g_o^s, \qquad g_e^s = \sum_{j>0} c_j \cos(j\theta), \qquad g_o^s = \sum_{j>0} s_j \sin(j\theta),$$

as done in Sect. 3. In the unstable case one has $g^u = g_c^u + g_e^u + g_o^u$ and $g_c^u = g_c^s$, $g_e^u = g_e^s$, $g_o^u = -g_o^s$, due to the symmetry as given in Sect. 2. Hence the *splitting function* is $g_o^u - g_o^s = -2g_o^s$. For simplicity we skip to mention the dependence in θ, μ, C when it is clear.

To do the Fourier analysis a number of equispaced values of θ in Σ (usually 2^{10} or 2^{11}) is taken and the values of q for the selected values of θ are obtained from the data computed in b) using 10 points Lagrange interpolation.

Once the Fourier representation of the first intersection of W_∞^s with Σ has been computed we can check different things:

A) To compare the computed values of g_c, c_1, c_2 and s_1, s_2 against the values derived in Sect. 3. To this end we use values of $C \geq 7.5$, computed with quadruple precision, to be closer to large C.

We remark that the computations in Sect. 3 have been done taking out the factor μ. Due to symmetry reasons (exchanging the role of the bodies) we should take also out a factor $1-\mu$. This is relevant for values of μ which are not small. Furthermore, in the case of odd harmonics, we should keep in mind that they become zero for $\mu = 1/2$, because in that case the problem is π-periodic instead of being 2π-periodic. This implies to take out a factor $1-2\mu$ for the odd harmonics.

In relation to this remark see details in [5] on the different factors which depend on μ in the harmonics. Note that in this reference terms containing μ^2 have not been computed.

B) For large C and μ away from 1/2 the dominant term in the splitting is s_1, the factor of $\sin(\theta)$. But for smaller values of C it can be a different harmonic. The function $g_o^s(\theta)$ can even be rather wild and contain several harmonics of similar amplitude. This affects also the number of primary homoclinic points for $\theta \in [0, 2\pi)$, beyond the obvious ones located at 0 and π.

To describe this phenomenology we shall look as the following items as depending on (μ, C):

1) The dominant term, that is the value of j which maximizes $|s_j|$,
2) How many terms must be taken to have an acceptable representation of g_o^s. For concreteness we take a value j such that $\sum_{1\leq i\leq j} |s_i| \geq 0.95 \sum_{1\leq i} |s_i|$,
3) How many zeros has g_o^s in a fundamental domain,
4) Special attention is also devoted to the changes in the function g^s and in the splitting which appear around the critical value $C_c = 32^{1/3}$.

In the results concerning the items in B) the values used for C go from $C = 7.5$ down, with step 0.01 while $g^s(\theta)$ behaves as a graph and for μ we use values of the form $\mu = 0.5 \times 10^{-0.01k}$ for $k = 0, \ldots, 300$. For the quadruple precision computations C ranges between 7.5 and 10 with step 0.1. Due to the fact that for $\mu = 1/2$ the coefficient s_1 is zero and s_2 is rather small, for $\mu = 1/2$ the selected range of C for quadruple precision computations has been taken as $[7.0, 8.5]$. Concerning μ the values taken for quadruple precision are as before but only for $k \equiv 0 \pmod 5$.

4.1 About the domain where expansions give a good approximation of W^s_∞

First the computed values of g_c, c_1, c_2 for different μ, C are scaled as follows, according to A)

$$\hat{g}_c = \frac{C^5}{\mu(1-\mu)} g_c, \quad \hat{c}_1 = \frac{C^{13}}{\mu(1-\mu)(1-2\mu)} c_1, \quad \hat{c}_2 = \frac{C^{11}}{\mu(1-\mu)} c_2. \tag{21}$$

The expected values of $\hat{g}_c, \hat{c}_1$ and $\hat{c}_2$ are, in the limit for large C, 32, 2^{18} and -9×2^{12}, respectively, according to Lemma 3.1. The results are shown in Fig. 1 using C as horizontal variable and the graphs of the scaled functions (21) for all values of μ together. The limit values are shown as horizontal lines. The behaviour of the different lines is compatible with the exponents of the remainder terms in Lemma 3.1. The left plot suggests that the subdominant term of $\hat{g}_c$ contains as factor, beyond $\mu(1-\mu)$, some other function depending on μ.

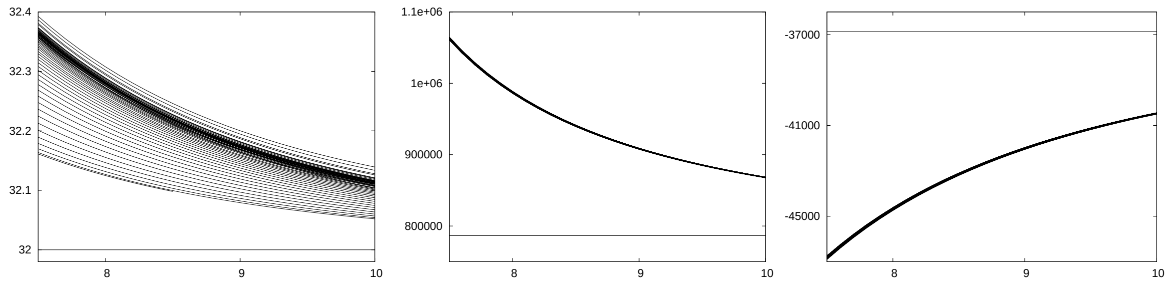

Figure 1: Computed values of $\hat{g}_c, \hat{c}_1$ and $\hat{c}_2$ for a large number of values of (μ, C) as a function of C. The values corresponding to all the μ values are plotted together. The horizontal lines correspond to the limit theoretical values according to Lemma 3.1.Left: Results shown for $\hat{g}_c$. Middle: For $\hat{c}_1$. Right: For $\hat{c}_2$.

Next we pass to the coefficients of the sinus terms. We shall consider s_1 and s_2 for all μ. It has been observed that beyond the contribution to s_2 given in Lemma 3.1, another term containing the factor $(\mu(1-\mu)(1-2\mu))^2 \exp(-C^3/12)$ (and hence zero for $\mu = 1/2$) is also present in the line of Remark 3.1. This suggests to do scalings of the form

$$\hat{s}_1 = \frac{-s_1 \exp(C^3/24)}{\mu(1-\mu)(1-2\mu)\sqrt{\pi C}/16},$$
$$\hat{s}_2 = \frac{s_2 \exp(C^3/12)}{\mu(1-\mu)C^{5/2}\sqrt{2\pi}/4}, \quad \hat{s}_2^* = \frac{s_2 \exp(C^3/24)}{(\mu(1-\mu)(1-2\mu))^2}, \tag{22}$$

where $\hat{s}_2$ is only used for $\mu = 1/2$ and $\hat{s}_2^*$ only for $\mu < 1/2$ (in the computations for $\mu < 0.45$). In the s_1 and s_2 cases we divide the numerically computed value by the dominant term given in Lemma 3.1. As shown in Fig. 2, left and middle, in both cases the results seem to tend to the unity. For s_1 all the computed values of $\mu < 1/2$ are plotted together, with excellent agreement between them.

The case of s_2^* is different. In the scaling we skip the exponential part and the factors depending on μ. To see the behaviour of the scaled variable both C and $\hat{s}_2^*$ are plotted in logarithmic scale. This shows a clear linear behaviour, with a slope close to -6, suggesting which should be the power of C of the dominant term of $\hat{s}_2^*$. For large values of C the term with $\exp(-C^3/24)$ is larger than the one with $\exp(-C^3/12)$ unless μ is close to 0 or to 1/2. This has been checked for $\mu \in (0.0001, 0.4998)$ and C greater than some $C(\mu)$ which ranges in $(6.8, 8)$. Note, however, than due to an extra $\mu(1-\mu)(1-2\mu)$ factor and to the evidence shown in Fig. 2 concerning the exponent of C, this additional contribution to s_2 is much less than s_1.

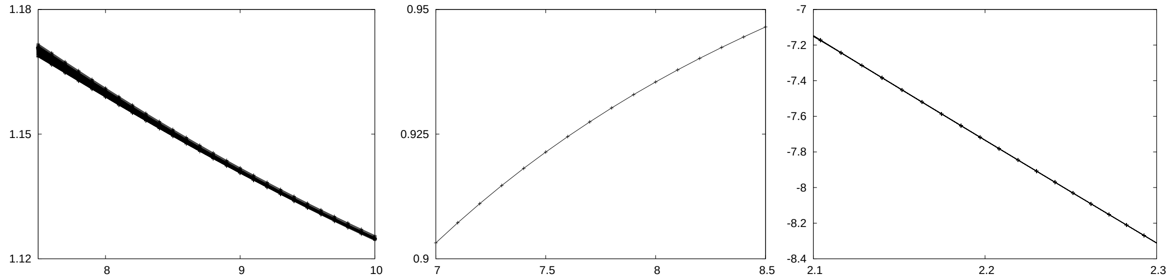

Figure 2: Left and middle: Plots of the scaled variables $\hat{s}_1$ and $\hat{s}_2$, defined in (22), as functions of C. They should tend to 1 when $C \to \infty$ according to Lemma 3.1. In the right plot $\log(\hat{s}_2^*)$ is plotted as a function of $\log(C)$ showing a nice close to linear behaviour which can be approximated by $\log(240) - 6\log(C)$ from a linear fit.

4.2 The splitting: Dominant and relevant terms, number of zeros

According to the points 1) to 3) in item B) we consider different aspects of the splitting in a large set of (μ, C) values. The results are shown in Fig. 3. In all the plots the horizontal variable is $\log_{10}(2\mu)$ with $\mu \in [0.0005, 0.5]$. The vertical variable is C. In the three plots it is observed that, for a given μ, the data stop at a given value of C. It corresponds to the value at which g^s is no longer a graph as a function of θ. Geometrically this means that the passage through $p = 0$ has a bifurcation and q passes from a local minimum to three nearby critical points.

On the left plot in Fig. 3 we display which is the dominant term in the splitting. The color code is: green if s_1 is dominant, blue if s_2 is dominant. Then magenta, light blue and yellow for s_3, s_4 and s_5 and, finally red for $s_j, j > 5$. To see the transition from dominant s_1 to s_2 one can use the expressions in Lemma 3.1 modified by Remark 3.1. It is found that it occurs for $\mu \approx (1 - aC^b \exp(-C^3/24))/2$ for a suitable coefficient, a, and exponent, b. Using the dominant terms one has $a = 4\sqrt{2}, b = 2$. As the values of C are moderate (except for values of μ exponentially close to $1/2$) the subdominant terms in Lemma 3.1 play a role. A fit of the data in Fig. 3 left gives $a \approx 0.416, b \approx 10/3$. Concerning the irregular behaviour near the critical value C_c of C see Sect. 4.3.

In the middle plot we show the number of harmonics that must be taken to have a good approximation, as defined in item B) point 2), to the shape of the splitting function $-2g_o^s$. The color code is similar to the one in the left plot with the exception that the case of 6 harmonics is shown in black and red is used for 7 or more harmonics. This shows that the shape of the splitting function becomes more and more wild when decreasing C.

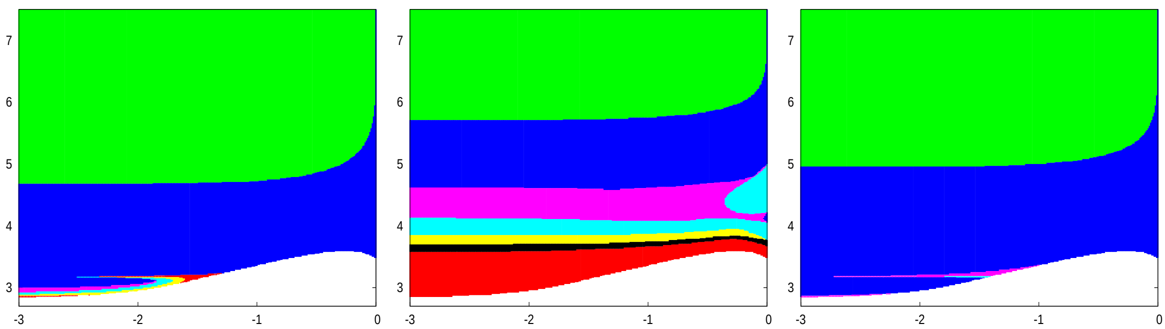

Figure 3: A plot of different characteristics of the splitting function as a function of the variables $(\log_{10}(2\mu), C)$. Left: the dominant term in the splitting. Middle: number of harmonics which are needed to have a good approximation of the function. Right: the number of zeros, i.e., primary homoclinic points. See the text for color code.

The right plot shows the number of zeros of the splitting function in $[0, 2\pi)$ which gives the number of primary homoclinic points in a fundamental domain. The color code is: green, blue, magenta and light blue for 2,3,6 and 8 zeros, respectively. Again see Sect. 4.3 for some details.

In the transition from 2 to 4 zeros which occurs near $C = 4.96$ for small μ a bifurcation is produced. To show it in Fig. 4 we plot the functions $g^s - g_c, g^u - g_c$ and the splitting function for $\mu = 0.5 \times 10^{-1.7} \approx 0.0099763$ and $C = 5.0, 4.9, 4.8$. On the left plot $g^s - g_c$ is plotted in red and $g^u - g_c$ in blue. Decreasing C the values of the plotted functions near $\theta = 0$ decrease, in agreement with the fact that the coefficient $|c_2|$ increases. One can observe that $g^s - g_c$ and $g^u - g_c$ exchange the position near $\theta = 0$. Accordingly the related splitting functions, shown in the right plot, pass from 2 zeros for $C = 5.0$ to 4 in the other cases.

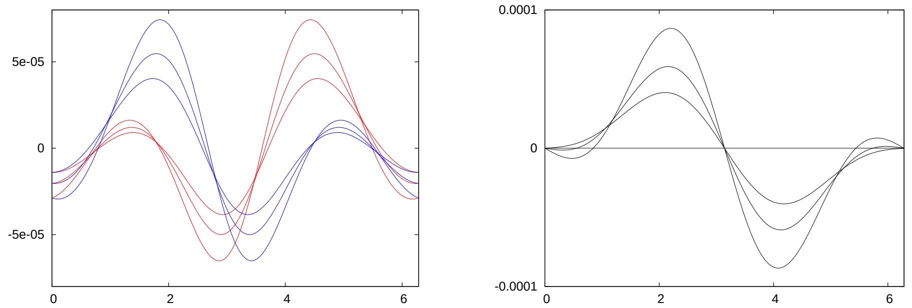

Figure 4: The vicinity of the bifurcation from 2 to 4 zeros for the splitting function for $\mu \approx 0.0099763$ and $C = 5.0, 4.9, 4.8$. Left: The functions $g^s - g_c$ (red) and $g^u - g_c$ (blue). Decreasing C the value of these functions on $\theta = 0$ decreases. Right: The corresponding splitting functions, with 2 zeros for $C = 5.0$ and 4 for $C = 4.9, 4.8$.

4.3 Near the critical C_c value

Now we discuss the anomalies near $C_c = 32^{1/3} \approx 3.1748$. To this end we have done computations as in Sect. 4.1 and 4.2 in a narrow strip in C from 3.15 to 3.37 with step 10^{-4}. Fig. 5 left and right are magnifications of Fig. 3 left and right, respectively. In the present domain the number of harmonics needed to have a good representation of the splitting function ranges from tens to more than one hundred.

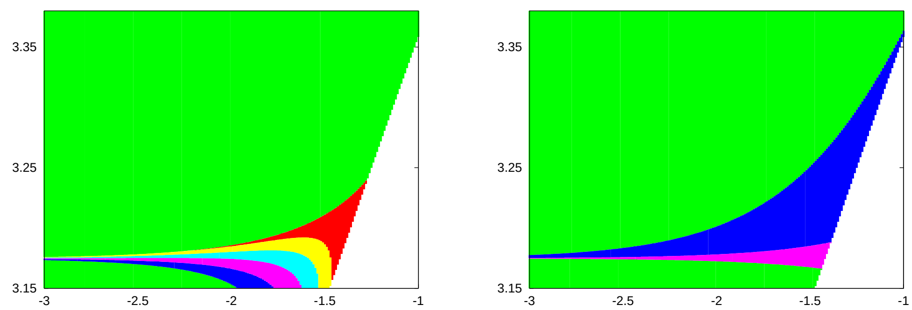

Figure 5: Results in a vicinity of the critical C_c value. Left: magnification of Fig. 3 left. The color code is now: green, blue, magenta, light blue, yellow and red for $j = 2, 4, 5, 6, 7$ and > 7, respectively. The white zone corresponds to places where g^s is not a graph wrt θ. Right: The number of zeros of the splitting function, where green, blue and magenta denote 4, 6 and 8 zeros, respectively.

As one can check from Fig. 5 three bifurcation lines appear, with changes from 4 to 6, from 6 to 8 and then from 8 to 4 in the number of zeros. In Fig. 6 we show first, on the left plot, the functions g^s and g^u for $\mu \approx 0.0099763$ and $C = 3.2$. For nearby values of C it is quite similar.

Up to 31 harmonics are requested to have a good representation of the splitting function for these parameter values. Note also that g^s and g^u are, relatively, quite close. On the middle and right plots the splitting function for the same value of μ used in the left plot and different values of C show the occurrence of bifurcations. The zero that has bifurcated from $\theta=\pi$, to the left of π in the middle plot, has moved close to $\theta=1.86$ in the right plot.

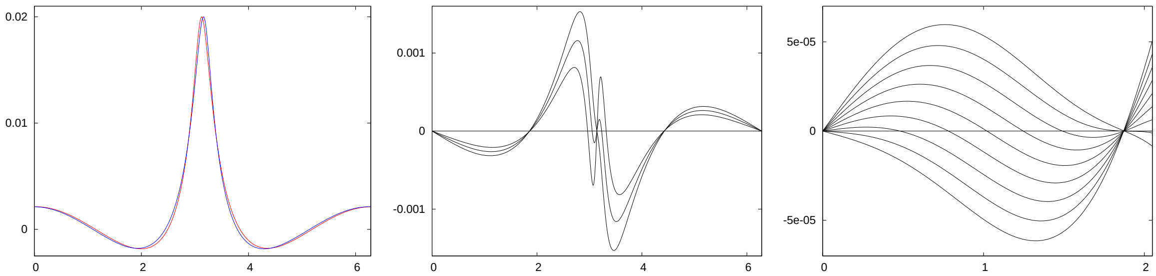

Figure 6: For $\mu=0.5\times10^{-1.7}$ and different values of C we show several phenomena. Left: The functions g^s (blue) and g^u (red) for $C=3.2$, displaying a sharp peak. Middle: The splitting function for $C=3.23, 3.22$ and 3.21. The absolute maxima decrease with C. Between 3.23 and 3.22 the number of zeros changes from 4 to 6. Right: A part of the splitting function for $C\in[3.168, 3.184]$ using 9 values with step 0.002. The corresponding curves can be identified by looking at $\theta=1$. When C decreases the value at $\theta=1$ increases. Between $C=3.182$ and $C=3.180$ a new zero emerges for θ close to zero (and the symmetric one near 2π), hence passing from 6 to 8. It moves to the right by decreasing C until 3 zeros coalesce and only 1 remains. The situation is symmetrical for $\theta>\pi$, giving the passage from 8 to 4.

As a final example of the effects near the critical C_c value, let us consider the evolution of the maximal value $||g^s||_\infty$ of g^s (that is, half the amplitude of the splitting function) when C changes. In Fig. 7 left for the value $\mu=0.5\times10^{-2.6}\approx0.0012559$ we plot $\log_{10}(||g^s||_\infty)$. For large C the amplitude increases when C decreases, as predicted by Lemma 3.1. A maximum occurs near $C=3.41$ with a value $\approx0.5576\times10^{-3}$. But then it decreases again until it reaches a value $\approx0.1244\times10^{-4}$ near $C=3.1789$. Decreasing again C the amplitude increases.

Looking at this phenomenon for other values of C one obtains a behaviour as shown in Fig. 7 right. For different values of μ one finds a local minimum of the amplitude as a function of C. All the minima occur for values of C close to C_c and tending to the critical value as $\mu\to0$.

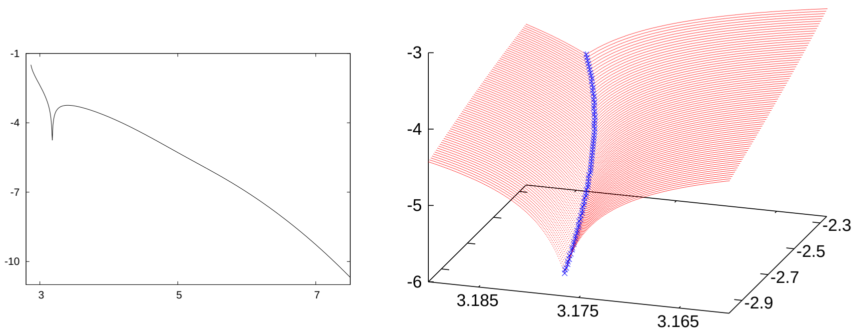

Figure 7: Evolution of the maximal amplitude of g^s (and, hence, of the splitting function) for fixed μ by changing C. Left: For $\mu\approx0.0012559$ we display the $\log_{10}$ of this amplitude as a function of C. Right: Evolution of these local minima in the (μ, C) plane in a 3D plot. The variables shown are $\log_{10}(2\mu)$ (in $[-3,-2.25]$), C (in $[3.16, 3.19]$) and the $\log_{10}$ of the amplitude. The location of the minima, marked in blue, shows that for $\mu\to0$ one has $C\to C_c$.

5 Return maps, simplified models and applications

Once the behaviour of the intersection of the manifolds $W^{s,u}_\infty$ with Σ is known, a common approach is to try to derive a return map to Σ, to obtain information on the dynamics based on that map.

Typically one obtains a separatrix-like map. Then one can try to approximate it by a standard-like map in a suitable domain and derive dynamical information. Classical references for that approach can be found, for instance, in [18, 1, 17, 14] and references therein. In [8] there is a presentation of the topic including several cases.

Two basic ingredients for a separatrix-like map are the return time and the splitting of separatrices. In the present problem we can take into account that, for large C, $W^s_\infty \cap \Sigma$ and $W^u_\infty \cap \Sigma$ are almost coincident. According to Lemma 3.1 and the results in Sect. 4.1, beyond the shift g_c of the pericentre wrt the two-body problem, the largest term is $c_2 \cos(2\theta)$ (both terms common to the two manifolds) and the splitting is due to s_1 (or s_2 for $\mu = 1/2$ and nearby) satisfying $|s_{1,2}| << |c_2|$. One can consider that $q = 4/C + g_c + g^s_e$ gives the location of the pericentre of the parabolic orbits for an integrable approximation of the RTBP. This approximation can be seen, for instance, as coming from the 1 dof Hamiltonian that is obtained by taking the time-2π map of the RTBP, i.e. passages through $t = 0 \pmod{2\pi}$, and using averaging.

This suggests to take as variables for the return map the angle θ and a radial variable defined as

$$Q = 4/C + g_c + g^s_e(\theta) - q. \tag{23}$$

That is, we measure Q from the average of the intersections of $W^{s,u}_\infty$ with Σ. Note that we are interested in values of q which are, in principle, less than $4/C + g_c + g^s_e(\theta)$. So Q will be positive. If the range of values of Q in which we are interested is relatively large compared to $g_c + g^s_e$, one can simply use $Q = 4/C - q$. When this done it will be explicitly mentioned.

For the return map we must estimate the return time. This is based on a modification of the two-body problem. Given Q we compute $q = 4/C - Q$, neglecting in (23) the g_c and g_e terms. Then we compute $r = 2/q^2$. If the sidereal energy is h we obtain $M = C/2 + h$ and, hence, the tangential velocity is $v = M/r$. We can rewrite the energy as

$$h = \frac{(C/2 + h)^2}{2r^2} - 1/r,$$

which gives an equation allowing to obtain $h(Q)$. If one wants to take into account the effect of the two bodies and the angle θ one can replace $1/r$ by $(1 - \mu)/r_1 + \mu/r_2$.

When h is known the return time (or period-like function) can be approximated as in the two-body problem by $T(Q) = 2\pi(-2h(Q))^{3/2}$. If Q is small and C is away from C_c one has the approximation for $h(Q)$ and $T(Q)$ as follows

$$h(Q) \approx \frac{4C^2 Q}{32 - C^3}, \qquad T(Q) \approx 2\pi \left(\frac{8C^2}{C^3 - 32}\right)^{-3/2} Q^{-3/2}. \tag{24}$$

Anyway we refer to [8] where it is studied, under quite general conditions, the return time after passing close to a parabolic fixed point. We can write a separatrix map as follows

$$Sep : \begin{pmatrix} \theta \\ Q \end{pmatrix} \mapsto \begin{pmatrix} \bar\theta = \theta + T(\bar Q) \\ \bar Q = Q + \sigma(\theta) \end{pmatrix}, \tag{25}$$

where here and in what follows σ denotes the splitting function, equal to $-2g^s_o$. As usual, one can localize around a given value Q_0 of Q and write $Q = Q_0 + \eta$. Neglecting terms in η^2 the map in (25) becomes

$$\begin{pmatrix} \theta \\ \eta \end{pmatrix} \mapsto \begin{pmatrix} \bar{\theta} = \theta + \alpha + \beta\bar{\eta} \\ \bar{\eta} = \eta + \sigma(\theta) \end{pmatrix},$$

where $\alpha = T(Q_0), \beta = |(dT/dQ)(Q_0)|$. Introducing $\xi = \alpha + \beta\eta$ we obtain, as usual, the standard-line map approximation

$$SM : \begin{pmatrix} \theta \\ \xi \end{pmatrix} \mapsto \begin{pmatrix} \bar{\theta} = \theta + \bar{\xi} \\ \bar{\xi} = \xi + \beta\sigma(\theta) \end{pmatrix}. \tag{26}$$

If we assume, as it happens for C large enough, that the dominant term in σ is of the form $\varepsilon \sin(\theta)$, see Fig. 3 left, where $\varepsilon = -2s_1$ (unless μ is very close to 1/2) we have the format of the classical standard map. Let be $\kappa = \beta\varepsilon$. As it is well known, invariant rotational curves (IRC) exist if $|\kappa| \leq \kappa_G \approx 0.971635$, Greene's value [4]. This requires, approximately,

$$3\pi \left(\frac{8C^2}{C^3 - 32}\right)^{-3/2} Q_0^{-5/2} \times 2\mu(1-\mu)(1-2\mu)\sqrt{\pi}C^{1/2} \exp(-C^3/24)/16 \leq \kappa_G.$$

In a simple case, C large so that $C^3 >> 32$ and μ small, one can derive an explicit bound for Q_0

$$Q_0 \geq \left(\frac{3}{\kappa_G}\right)^{2/5} \frac{\pi^{3/5}}{8} C^{4/5} \mu^{2/5} \exp(-C^3/60). \tag{27}$$

The prediction of the location of IRC given by (27) can be improved in different ways. If Q is not very small instead of the formulas in (24) given C and Q one can solve the equation for h exactly and then compute T and dT/dQ from that value of h. Another improvement can be done using the numerical results for ε obtained as mentioned in Sect. 4.1. Finally one can take into account in (26) more harmonics in σ. The case of the first two harmonics, as mentioned at the Introduction, leads to add an additional parameter and σ depends on a "shape parameter" γ and an "amplitude parameter" ε. Then one has to replace κ_G by some $\kappa_G(\gamma)$ in (27).

6 Numerical computation of the boundaries of bounded motion

It is possible to compute when IRC start to show up at some distance of the splitted separatrix. They give boundaries for the existence of bounded motion, letting aside the little periodic islands which appear between the splitted separatrix and the IRC. The computations have been done using the equations coming from (1) so that when the body of negligible mass is far away the equations are very smooth with a tiny periodic perturbation. Then the values of r at the pericentre passages are changed to q and to Q.

A simple algorithm, given values of (μ, C), is as follows:

1) Take initial conditions on $\theta = 0$ for values of r of the form $r_0 + k\Delta r, k \geq 0$, where r_0 it is taken slightly larger than the value r_p of the two-body pericentre. Concerning Δr: Given r one can estimate the corresponding return time $T(r)$ using a variant of (24). Then one can determine a value $\bar{r} > r$ such that $T(r) - T(\bar{r}) = 2\pi$. That is, the return requires one less revolution. One takes $\Delta r = (r - \bar{r})/L$, where L is taken initially equal to 20 or similar and in further refinements one takes larger values as 60 and 200.

2) Given initial conditions the equation of motion are integrated using high order Taylor method. If $r(t)$ becomes large enough we check if the current point can be considered to be at the outer part of W^s_∞, leading to escape. In this case the initial point is discarded. The variational equations in vector form with random normalized initial conditions, ξ_0 are

also integrated. This allows to check if the orbit can be considered non-regular, stopping soon the computations for that initial r. One has to keep in mind that, even in the case of a foliation by regular orbits, the twist-like condition dT/dr can have a large absolute value. This leads to nearly linear increase like $\alpha_0 + \alpha_1 t$ for $||\xi(t)||$. If α_1 is below some computable bound the initial point should not be discarded.

3) When the number of returns reaches some value (e.g., multiples of 1000) one can check if the computed iterates of the Poincaré map can be assumed to be in an island. This can be done by an estimate of the rotation number (a rational with relatively small denominator) and by looking at the projection of the iterates on its angular component and detecting the existence of relatively large gaps.

4) If the computation of Poincaré iterates proceeds in a smooth way, when reaching a given number of iterates N (typically $N = 10^4$ or 2-5 times that value) the rotation number ρ of the candidate to invariant curve is computed. A method based only on topological order of the angles, see e.g. the Appendix in [12] is used. The method provides lower and upper estimates of ρ. One checks if the difference is below some tolerance (of the order of a/N^2 a being a moderate value like 5 or 10) and the estimated ρ is not too close to a rational with relatively small denominator, it is accepted that the initial point belongs to an IRC.

The previous algorithm has been applied to different values of C for a sample of values of μ of the form $\mu_k = 0.5 \times 10^{(-0.05k)}, k = 0, 1, \ldots, 60$. The results are reported in Figs. 8 and 9. In Fig. 8 we consider the cases of small C: $C = 3.5$ and $C = 4.0$. We display the value of Q simply taken as $Q = 4/C - q$. For $C = 3.5$ values close to $\mu = 1/2$ are missing. They belong to the white set in Fig. 3 correspond. That is $W^s_\infty \cap \Sigma$ is no longer a graph.

The results for constant C show that decreasing μ, as the amplitude of the splitting decreases, the value of Q also decreases. Concerning the average return time to the Poincaré section it increases as μ decreases. Note that in the case $C = 3.5$ and also in the case $C = 4$ for μ large, the values of the return time when they change from a value μ_k to the one for μ_{k+1} are close to the same integer or the integer increases by one.

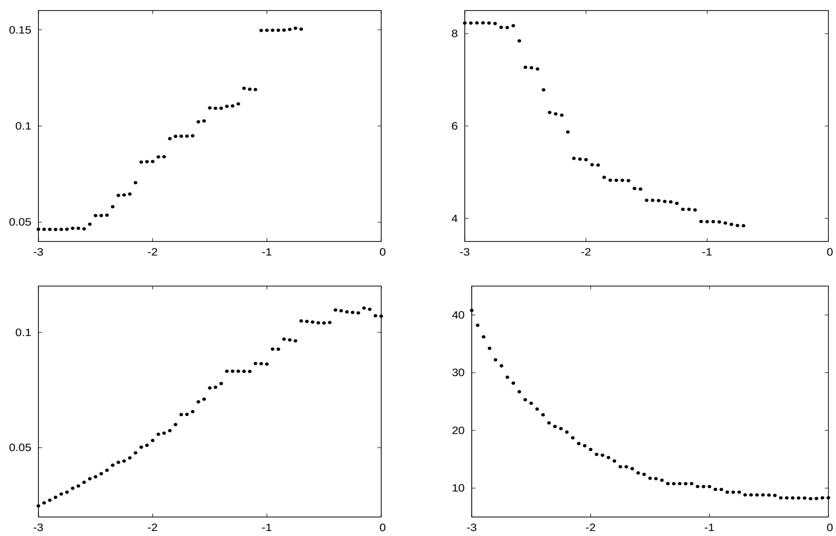

Figure 8: Results on the place where IRC start to be found. Up: for $C = 3.5$. Down: for $C = 4.0$. Left: Values of Q as a function of μ. Right: Values of the average return time to Σ, $T(Q)$, measured in revolutions of the primaries. The horizontal variable is $\log_{10}(2\mu)$.

Fig. 9 shows the cases $C = 5.5$ and $C = 6.0$. Last one requires somewhat too long computations, see the related values of $T(Q)$ on the right lower plot. The values of g^s_c and g^s_e agree quite well with Lemma 3.1 and are negligible at the scale of the left plots. The results for both Q and $T(Q)$ are quite smooth. Furthermore one checks from the data (Fig. 9 right) that, for $\mu < 0.1$, $T(Q)$ is proportional to Q^{ν} with $\nu \approx -1.45$ for $C = 5.5$ and $\nu \approx -1.49$ for $C = 6.0$, approaching the theoretical value $-3/2$ given in (24).

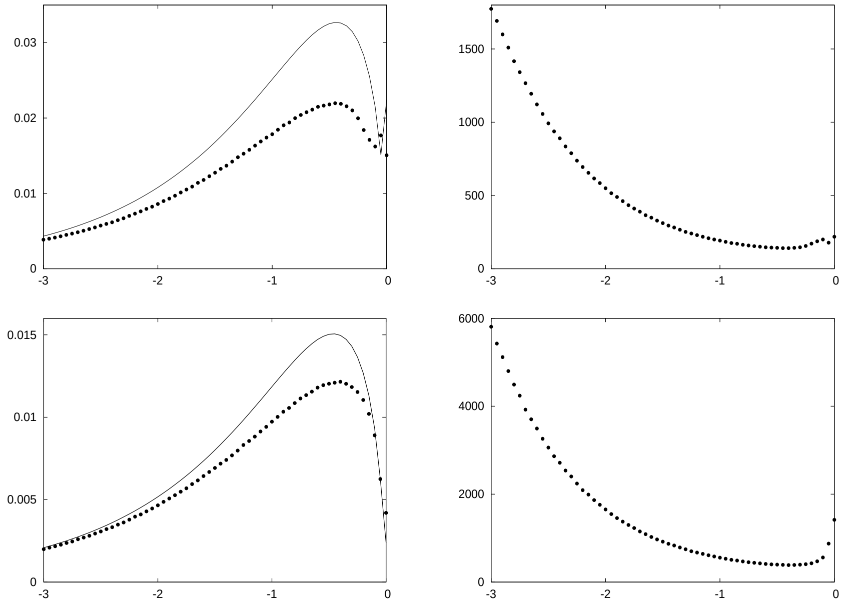

Figure 9: Results on the place where IRC start to be found. Up: for $C = 5.5$. Down: for $C = 6.0$. Left: Values of Q as a function of μ. Right: Values of the average return time to Σ, $T(Q)$, measured in revolutions of the primaries. The horizontal variable is $\log_{10}(2\mu)$. The continuous lines show the theoretical values based on a classical standard map approximation.

The continuous lines in the left plots give the theoretical predictions on the value of Q when IRC start to appear, using the improvements mentioned at the end of Sect. 5 but assuming that only the term in $\sin(\theta)$ plays a role in the splitting function σ. According to Fig. 3 this is acceptable for $C = 6$ but not for $C = 5.5$, for which the second harmonic is also relevant. Anyway, the relative difference between this prediction and the computed behaviour decreases when μ approaches 0 and improves from $C = 5.5$ to $C = 6$. Next we present an argument to explain this anomaly.

Taking for granted that only the first harmonic is relevant in the splitting function, so that $\sigma = \varepsilon \sin(\theta)$ the basis for the prediction of the apparition of IRC is $|(dT/dQ)(Q_0)|\varepsilon \le \kappa_G$, as used in (26, 27). Hence, given ε and a decreasing return time function $T(Q)$ one has to look for the first value of Q_0 such that $|(dT/dQ)(Q_0)| \le \delta := \kappa_G/\varepsilon$. If T as a function of Q behaves in the form $T = \Gamma Q^{-3/2}$ as in (24), where Γ is a constant depending on C, the function $|dT/dQ|$ is monotonically decreasing when Q increases going away from 0.

Now assume that $T(Q)$ contains also a fast oscillation of small amplitude for $Q > 0$ close to 0. As a toy model we consider $T(Q) = Q^{-3/2} + 2Q^{1/2}\sin(Q^{-3/2})$. Due to the oscillations it can happen that $|dT/dQ|$ reaches the value δ for some $Q_0^* < Q_0$. Indeed this happens and it is easy to prove, in this toy model, that the relative error $1 - Q_0^*/Q_0$ behaves as $\delta^{-1/5}$. This would explain why the apparition of IRC in Fig. 9 occurs before the theoretical expectation and also why the relative error decreases when μ decreases (and, hence, ε decreases and δ increases).

An evidence of the existence of these oscillations is shown in Fig. 10. For $\mu = 0.1, C = 6$ the algorithm at the beginning of this section has been applied. The left plot shows the orbits of several initial points, either chaotic or around islands (in red) or detected as IRC (in blue). The value plotted is Q, using the simple version $4/C - q$, as a function of θ. For completeness we also plot in black the function $g_c^s + g_e^s(\theta)$ but using the variable $Q + 0.01177$. That is, the true location of this function has negative values of $4/C - q$. The plot gives evidence that the shape of the IRC is very similar to $g_c^s + g_e^s(\theta)$, moving up in Q.

On the left plot one can guess two similar *layers* and, in particular, islands around elliptic fixed points located at $\theta = 0$. For instance, the fixed point on the lower layer, near $Q = 0.01142$ corresponds to a periodic orbit such that the return to the pericentre is produced after 434 revolutions of the primaries. Only the boundaries of these islands are shown. Many similar layers are found below these two, with chaotic orbits and islands of different periods, but no evidence of IRC. When the initial data are taken close to $g_c^s + g_e^s(\theta)$ the dynamics is mostly chaotic.

The right plot shows a portion of a layer on top of the ones in the left plot. The fixed elliptic point returns to Σ after 407 revolutions of the primaries. From the values of Q we have subtracted a function $Q_a(\theta)$ to keep the average close to zero. This function $Q_a(\theta)$ is rather close (except by the addition of a constant term) to $g_c^s + g_e^s(\theta)$. Different IRC can be seen in the plot. But despite initial data on $\theta = 0$ are taken equispaced in r, the average distance between IRC has fluctuations and this implies anomalies in the function $T(Q)$. This is the kind of phenomenon that we have considered in the toy model and which is related to the differences between theoretical predictions and observed behaviour in Fig. 9.

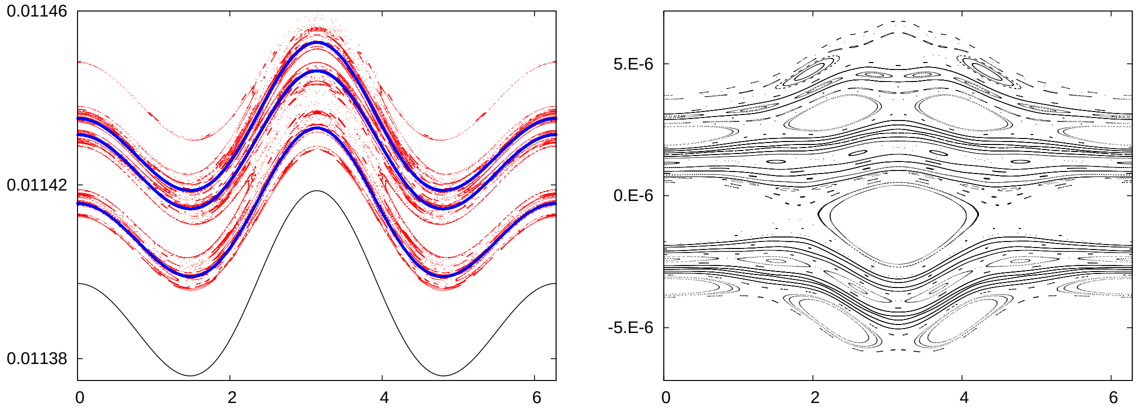

Figure 10: Left: For $\mu = 0.1, C = 6$ an example of iterates of orbits of the Poincaré map associated to Σ, including some of the first IRC (the ones with minimal Q) found in that case. The variables plotted are $(\theta, Q = 4/C - q)$. A plot of $g_c + g_e^s(\theta)$, shifted up by 0.01177 is also shown in black. Right: The dynamics in one the *layers* modified to skip the large oscillations of the layers.

7 Conclusions

In this work we have studied for the planar circular RTBP and a large set of values of the mass ratio μ and the Jacobi constant C, two main topics:

- The behaviour of the invariant manifolds of the periodic orbit at infinity, including the related splitting, both theoretically and numerically. This allows to determine the domain of applicability of the theory in the (μ, C) variables and which type of phenomena occur outside that domain.

- Given a suitable Poincaré section we have derived return maps from the information provided by the return time and the splitting. From this it is possible to predict where one can expect to have invariant rotational curves confining the motion.

Some exceptional phenomena, either concerning the splitting or the IRC have been detected and several explanations have been proposed.

A similar methodology can be applied to a variety of problems to obtain realistic bounds allowing to locate the place where it can be guaranteed that the motion will be bounded.

Appendix

In this Appendix we sketch the computation of the coefficients $a_j(\theta)$ of the invariant manifold (7).

Given some values of μ, C, we can eliminate the variable ω in the equations using the Jacobi integral. To do that it is useful to introduce $W = \omega - C/2$ (i.e., the sidereal energy). Then (5) becomes

$$W = \frac{1}{2}p^2 - \frac{1}{2}q^2 + \frac{1}{2}q^2(1-\sigma_1) + \frac{1}{8}q^4\left(\frac{C}{2} + W\right)^2 \tag{28}$$

and (4) can be written as

$$\begin{aligned} \dot{q} &= -\frac{1}{4}q^3 p, \\ \dot{p} &= -\frac{1}{4}q^4\sigma_3 + \frac{\mu(1-\mu)}{8}q^6\sigma_2\cos\theta + \frac{q^6}{8}\left(\frac{C}{2}+W\right)^2, \\ \dot{\theta} &= -1 + \frac{1}{8}q^4 C + \frac{1}{4}q^4 W. \end{aligned} \tag{29}$$

To obtain the invariant manifolds we look for

$$p = F(q,\theta) = \sum_{j\geq 1} a_j(\theta)q^j, \qquad W = G(q,\theta) = \sum_{j\geq 2} w_j(\theta)q^j,$$

where $a_j(\theta), w_j(\theta)$ are periodic functions in θ. The coefficients $a_j(\theta), w_j(\theta)$ are obtained by solving the following invariance equation

$$\dot{p} = \dot{q}\frac{\partial F}{\partial q} + \dot{\theta}\frac{\partial F}{\partial \theta}, \tag{30}$$

using (29), together with (28).

For a given periodic function $g(\theta)$ it will be convenient to split it as $g(\theta) = \bar{g} + \tilde{g}(\theta)$ where $\bar{g}$ is constant and $\tilde{g}$ purely periodic in θ. In particular we shall write $a_j(\theta) = \bar{a}_j + \tilde{a}_j(\theta)$.

It is clear that $a_1(\theta) = 1$ for the stable manifold, and $a_1(\theta) = -1$ for the unstable one. Next coefficients are obtained in a recurrent way by solving (30) and (28).

The first coefficients are easily obtained as

$$\begin{gathered} a_2(\theta) = a_4(\theta) = a_6(\theta) = 0, \quad a_3(\theta) = -\frac{C^2}{32a_1}, \quad a_5(\theta) = \frac{1}{2a_1}\left(\frac{\mu(1-\mu)}{2^4} - a_3^2\right), \\ \tilde{a}_7(\theta) = 0, \quad \tilde{a}_8(\theta) = \frac{9\mu(\mu-1)}{2^7}\sin(2\theta), \quad \tilde{a}_9(\theta) = 0, \\ w_2(\theta) = w_3(\theta) = w_4(\theta) = w_5(\theta) = 0, \quad w_6(\theta) = -\frac{3\mu(1-\mu)}{32}\cos(2\theta), \quad w_7(\theta) = 0 \end{gathered}$$

and for $n \geq 10$ we obtain the following recurrences

$$\begin{aligned} \bar{a}_{n-3} &= \frac{4}{a_1(n-2)}\bar{\mathcal{T}}_n & (31) \\ \tilde{a}'_n(\theta) &= \frac{C}{8}a'_{n-4}(\theta) - \frac{n-2}{4}a_1 a_{n-3}(\theta) + \mathcal{T}_n, & (32) \\ a_{n-3}(\theta) &= \bar{a}_{n-3} + \tilde{a}_{n-3}(\theta), & (33) \\ w_{n-2}(\theta) &= \frac{1}{2}\mathcal{A}_{n-2} + \frac{C}{8}w_{n-6} + \frac{1}{8}\mathcal{D}_{n-6} + \mathcal{G}_{n-2}, & (34) \end{aligned}$$

where $' = d/d\theta$ and

$$\begin{aligned}
\mathcal{T}_n &= -\frac{1}{4}\mathcal{S}_{n-2} + \frac{1}{4}\mathcal{R}_n - \frac{1}{8}(Cw_{n-6} + \mathcal{D}_{n-6}) + \mathcal{F}_n, \\
\mathcal{S}_m &= \sum_{j=2}^{m-2}(m-j)a_j a_{m-j} = \sum_{j=3}^{m-3}(m-j)a_j a_{m-j}, \\
\mathcal{R}_m &= \sum_{j=6}^{m-1} w_{j-4}a'_{m-j} = \sum_{j=8}^{m-1} w_{j-4}a'_{m-j}, \\
\mathcal{D}_m &= \sum_{j=2}^{m-2} w_j w_{m-j} = \sum_{j=6}^{m-2} w_j w_{m-j}, \\
\mathcal{A}_m &= \sum_{j=1}^{m-1} a_j a_{m-j}.
\end{aligned}$$

Moreover, if m is odd then $\mathcal{F}_m = \mathcal{G}_m = 0$ and for $m = 2l$

$$\mathcal{F}_{2l} = -\frac{\delta_{l-2}}{4}[-C_{l-2}^{(3/2)}(\xi) + \xi C_{l-3}^{(3/2)}(\xi)], \qquad \mathcal{G}_{2l-2} = -\frac{\delta_{l-2}}{2}C_{l-2}^{(1/2)}(\xi),$$

where $C_n^{(\alpha)}$ denotes the Gegenbauer polynomial of degree n, $\xi = \cos\theta$ and

$$\delta_m = \frac{1}{2^m}((1-\mu)\mu^m + (-1)^m\mu(1-\mu)^m).$$

We note that at each step $n \geq 10$ we can assume that the following coefficients are known

$$a_1, a_2, \ldots, a_{n-4}, \quad \tilde{a}_{n-3}, \tilde{a}_{n-2}, \tilde{a}_{n-1}, \quad w_2, \ldots w_{n-3}.$$

Then $\bar{a}_{n-3}$ is given by (31). In this way the coefficient a_{n-3} is completely determined from (33). Moreover the periodic part of a_n is computed by integration from (32). Finally we compute w_{n-2} using (34).

Using the recurrences (31-34) and an induction argument it is easy to prove the properties given in the following Lemma.

Lemma 7.1.

1. *If $n = 2k$, then $a_n(\theta)$ is an odd function with terms $\sin(j\theta)$ for $j = 1, 2, \ldots, k-2$, $j \neq k-3$.*
2. *If $n = 2k+1$, then $a_n(\theta)$ is an even function with terms $\cos(j\theta)$ for $j = 1, 2, \ldots, k-4, k-3$. Moreover $\bar{a}_n$ is a polynomial in C of degree $n-1$.*
3. *The coefficient $w_n(\theta)$ has the same parity as n.*

Acknowledgments

This work has been supported by grants MTM2010-16425 and MTM2013-41168 (Spain), 2009 SGR 67 and 2014 SGR 1145 (Catalonia). The authors are indebted to Amadeu Delshams, Àngel Jorba and Arturo Vieiro for helpful discussions. A massive use has been made of the computing facilities of the UB Dynamical System Group and the technical support of Jaume Timoneda is deeply acknowledged.

References

[1] B.V. Chirikov, A universal instability of many-dimensional oscillator systems. *Phys. Rep.*, 52:264–379, 1979.

[2] A.M. Fox and J. Meiss, Critical invariant circles in asymmetric and multiharmonic generalized standard maps. *Commun. Nonlinear Sci. Numer. Simult.*, 19:1004–1026, 2014.

[3] J. Galante and V. Kaloshin, Destruction of invariant curves in the restricted circular planar three-body problem by using comparison of action. *Duke mathematical Journal*, 159:275–327, 2011.

[4] J.M. Greene, A method for determining stochastic transition. *J. Math. Phys.*, 6:1183–1201, 1979.

[5] M. Guardia, P. Martín and T. M.Seara, Oscillatory motions for the restricted planar circular three-body problem. Preprint available at `http://arxiv.org/abs/1207.6531`, 2014.

[6] J. Llibre and C. Simó, Oscillatory solutions in the planar restricted three-body problem. Math. Ann., 248:153–184, 1980.

[7] R. Martínez and C. Pinyol, Parabolic orbits in the elliptic restricted three-body problem. *Journ. Diff. Equations*, 111:299–339, 1994.

[8] R. Martínez and C. Simó, Return maps, dynamical consequences and applications. Preprint, 2014.

[9] R. Martínez and C. Simó, Regularity of the infinity manifolds and global dynamics in the Sitnikov problem. In preparation, 2014.

[10] R. McGehee, A stable manifold theorem for degenerate fixed points with applications to Celestial Mechanics. *J. of Differential Equations*, 14:70–88, 1973.

[11] J. Moser, *Stable and Random Motions in Dynamical Systems.* Annals of Mathematics Studies, Princeton Univ. Press 1973.

[12] J. Sánchez, M. Net and C. Simó, Computation of invariant tori by Newton-Krylov methods in large-scale dissipative systems. *Physica D*, 239:123–133, 2010.

[13] C. Simó Analytical and numerical computation of invariant manifolds. In *Modern methods in celestial mechanics*, D. Benest and C. Froeschlé, editors, pp. 285–330, Editions Frontières, 1990. (also available at `www.maia.ub.es/dsq/2004`, number 2).

[14] C. Simó and D. Treschev, Stability islands in the vicinity of separatrices of near-integrable symplectic maps. *Discrete and Continuous Dynamical Systems B*, 10:681–698, 2008.

[15] K.A. Sitnikov, The existence of oscillatory motions in the three-body problems. *Soviet Physics Doklady*, 5:647650, 1960.

[16] V. Szebehely, *Theory of orbits.* London,New York: Academic Press 1967.

[17] D. Treschev, Multidimensional symplectic separatrix maps. *J. Nonlinear Sci.*, 12:27–58, 2002.

[18] G.M. Zaslavskii and B.V. Chirikov, Stochastic instability of non-linear oscillations. *Soviet Physics Uspekhi*, 14:549–568, 1972.